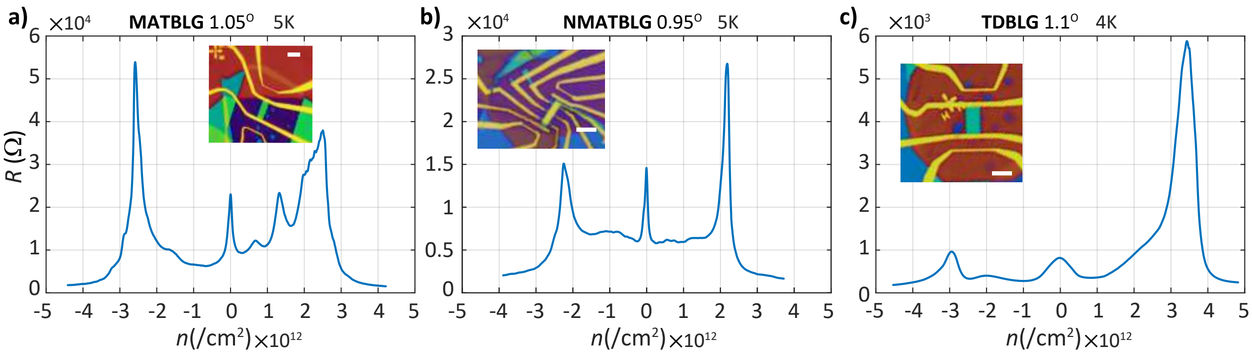

Extended Data Fig. 1: Resistance response as a function of density (n): (a), **(b)**, and **(c)**, Resistance as a function of density for MATBLG (at 5K), near-MATBLG (at 5K) and TDBLG (at 4K), respectively. For all three devices, we have used the full-filling ($\nu = \pm 4$) carrier density (n_s) to measure the twist angle (θ) using $n_s = 8\theta^2/\sqrt{3}a^2$, where $a = 0.246nm$ is the lattice constant of monolayer graphene. For MATBLG, near-MATBLG and TDBLG $n_s \approx 2.58 \times 10^{12}, 2.15 \times 10^{12}$ and $3.19 \times 10^{12} cm^{-2}$ respectively, which translates to $\theta \sim 1.05^0, 0.95^0$ and 1.1^0 respectively. Inset shows the optical images of the corresponding devices. The scale bars are $5\mu m$.

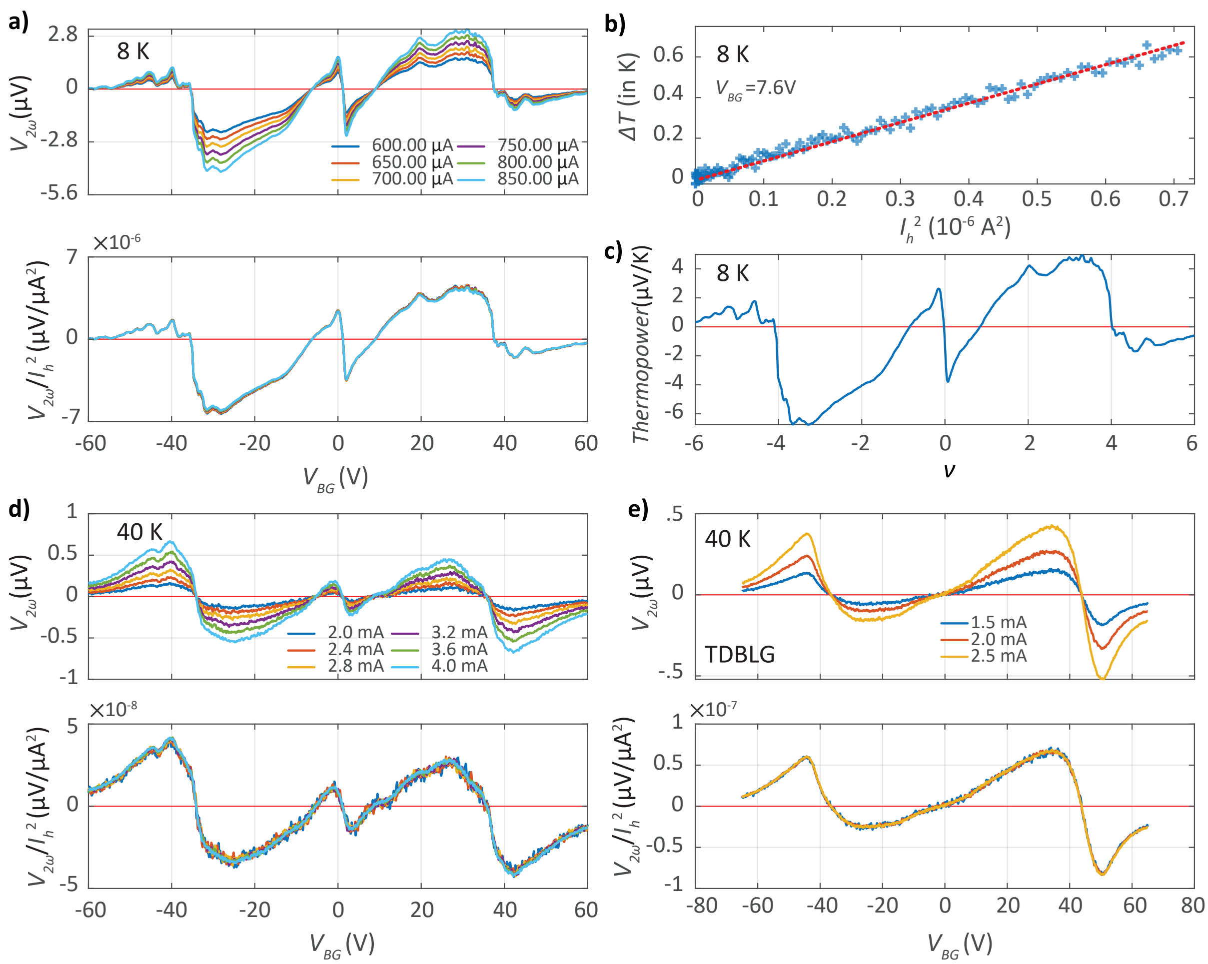

Extended Data Fig. 2: The linear regime of thermopower measurement: (a) V$_{2\omega}$ signal versus V_{bg} for different applied heater currents (I_h), respectively, at 8K for MATBLG device (top panel). V$_{2\omega}$ signal normalized by the squire of respective heater currents (I_h^2) versus backgate voltage V_{bg} (bottom panel). All the normalized $V_{2\omega}/I_h^2$ values overlap well showing the $V_{2\omega}$ measurements have been performed in the linear response regime. **(b)** Measured temperature difference (ΔT) as a function of I_h^2 at 8K at backgate voltage $V_{bg} = 7.6V$. Within the maximum heater current range, a clear linear trend (dashed red line) can be observed between ΔT and I_h^2, and $\Delta T << T$. **(c)** Thermopower as a function of filling ν derived from measured V$_{2\omega}$ signal and ΔT. **(d), (e)** (Top panels) V$_{2\omega}$ signal versus V_{bg} for different applied heater currents (I_h), at 40K for MATBLG and TDBLG device, respectively. (Bottom panels) V$_{2\omega}$ signal normalized by the squire of respective heater currents (I_h^2) versus V_{bg}, both showing linear regime behavior.

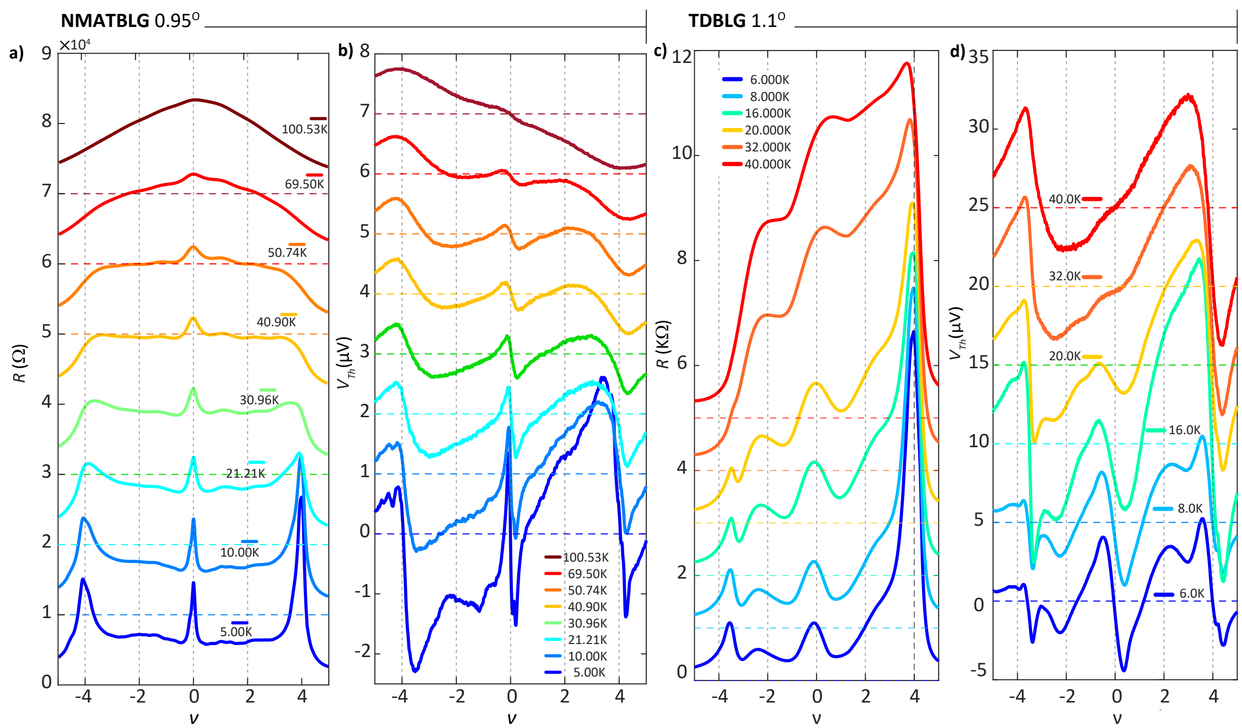

Extended Data Fig. 3: Resistance (R) and thermoelectric voltage (V_{Th}) response for near MATBLG abd TDBLG device: (a),(b), R and V_{Th} response of near MATBLG device, as a function of ν at different temperatures, depicted in a shifted plot. The horizontal lines represent the zero reference at each temperature. R remains featureless at integer fillings, except for the Dirac point and $\nu = \pm 4$. The V_{Th} closely resembles that of MATBLG, exhibiting similar crossing points near $\nu \approx \pm 1$. However, in comparison to MATBLG, these crossing points near $\nu \approx \pm 1$ show some variation with T and persist only up to $50K$. Beyond $100K$, V_{Th} as well as R begins to resemble a graphene-like spectrum. **(c),(d)**, R and V_{Th} response of TDBLG device, as a function of ν at different temperatures. In contrast to MATBLG or 0.95^o near MATBLG, the additional crossing points in the band vanish at a much lower temperature, around $20K$. Distinctively, above $20K$, V_{Th} remain completely positive (negative) in the conduction (valence) band, which is opposite to how V_{Th} behaves for MATBLG and near MATBLG devices, but resembles semi-classical thermopower S_{SC} behaviour shown in Extended Data Fig. 4e.

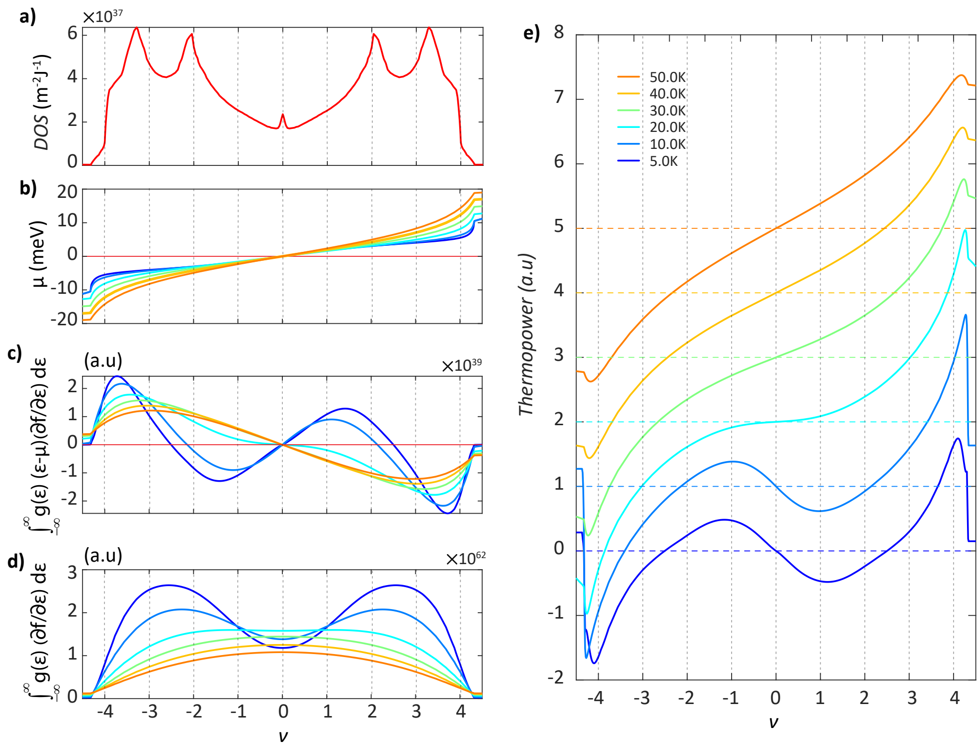

Extended Data Fig. 4: Theoretical calculations of semiclassical thermopower : (a) Continuum model DOS (by Zondiner, U. et al.) as a function of filling (ν) corresponding to twisted bilayer with twist-angle 1.05^0. **(b)** Self-consistently solved chemical potential (μ) as a function of ν at different temperatures. **(c)** and **(d)**, respectively, show the numerator and denominator of Eq.1 in method section as a function of ν at different temperatures. **(e)** Semi-classical thermopower with ν at different temperatures plotted with an offset of 1 unit. The dashed horizontal lines correspond to the zero line references for respective temperatures.

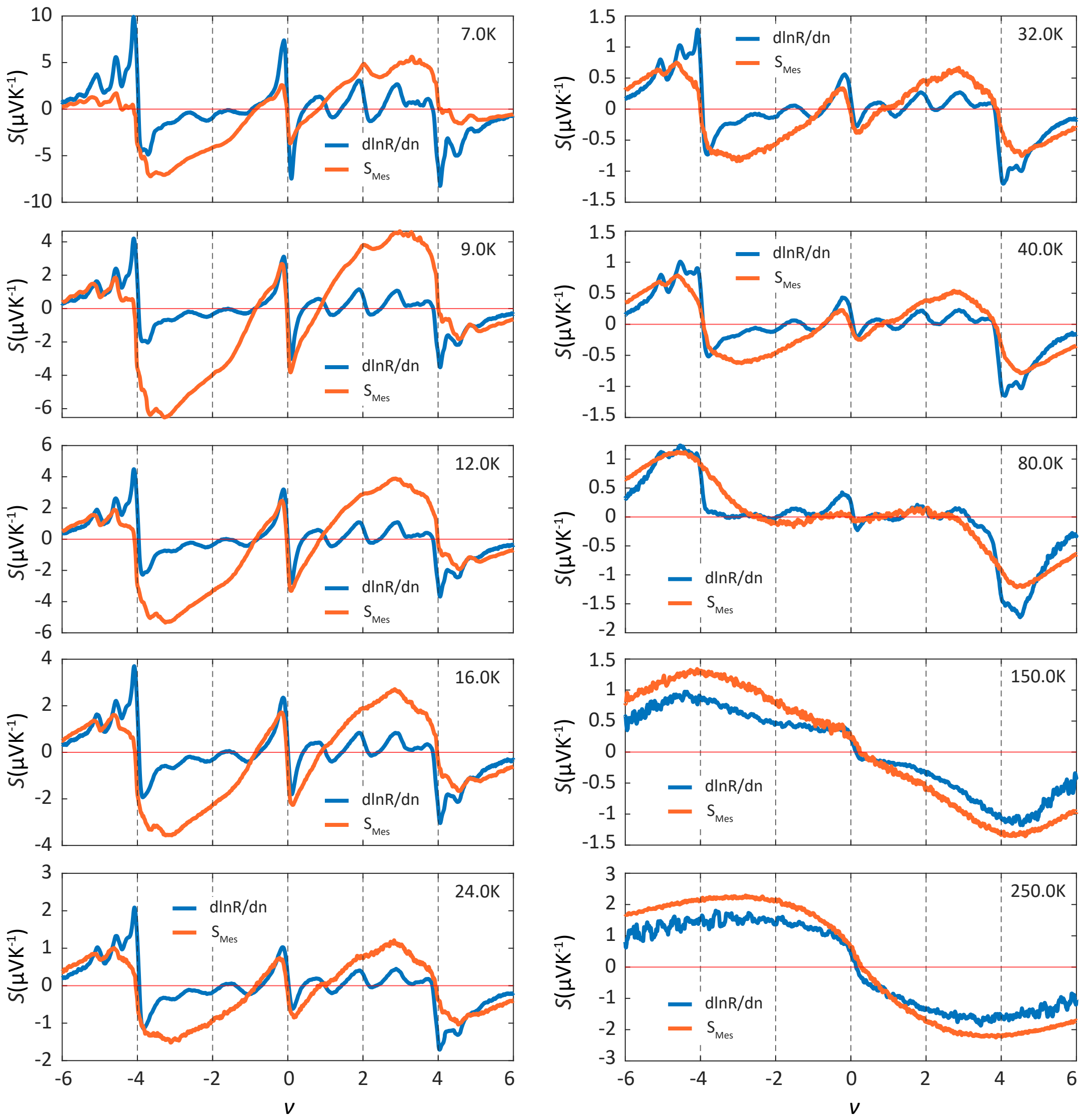

Extended Data Fig. 5: Comparison between $dln(R)/d\nu$ and measured V_{Th} for MATBLG device: Comparison between measured V_{Th} signal and $dln(R)/d\nu$ (both scaled to arbitrary units for visual clarity) at different temperatures. Blue and orange lines present the $dln(R)/d\nu$ and V_{Th}, respectively. Below $T < 120K$, the measured thermopower (in orange solid line) lacks many of the crossing points predicted by $dln(R)/d\nu$ (in blue solid line). Above $120K$ the V_{Th} matches well with Mott relation with a graphene-like thermopower spectrum.

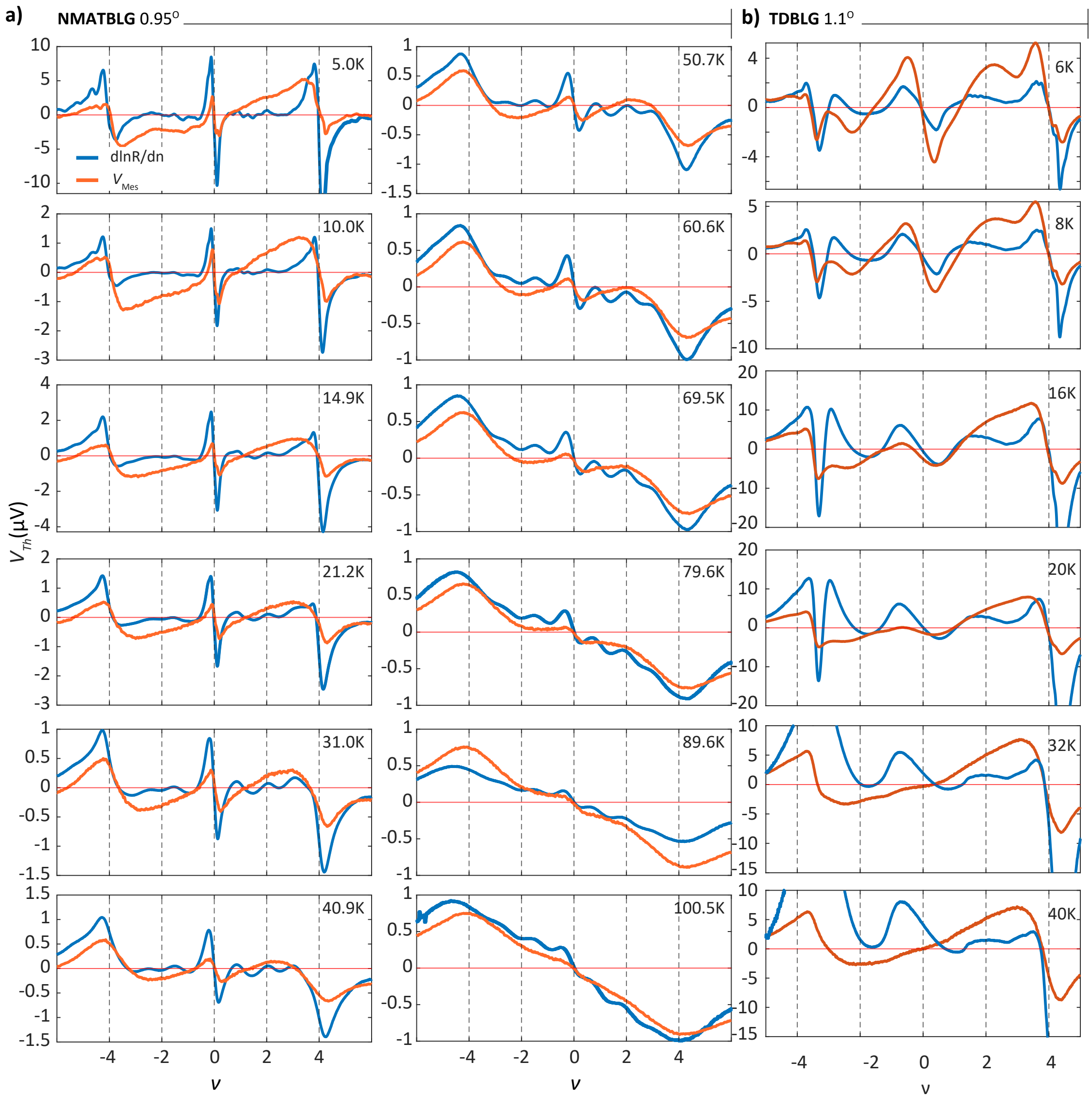

Extended Data Fig. 6: Comparison between $dln(R)/d\nu$ and measured V_{Th} for near MATBLG and TDBLG devices: (a), (b), Comparison between measured V_{Th} signal and $dln(R)/d\nu$ (both scaled to arbitrary units for visual clarity) at different temperatures for near MATBLG and TDBLG device, respectively. Blue and orange lines present the $dln(R)/d\nu$ and V_{Th}, respectively. Mott violation can also be observed in near MATBLG devices. Below $50K$, V_{Th} is generally more symmetric between the valence and conduction band, showing only one crossing point for each conduction and valence band, whereas, $dln(R)/d\nu$ shows many crossing points. Here also, the measured V_{Th} matches quite well with $dln(R)/d\nu$ at higher temperatures ($> 90K$). In TDBLG, there is a distinct departure of the V_{Th} behaviour as compared to the MATBLG and near-MATBLG devices. At low temperatures ($< 20K$), V_{Th} shows qualitative agreement with $dln(R)/d\nu$ in terms of general peak and the number of zero crossing points (in the conduction band). At larger temperatures, the asymmetry in R (see Extended Data Fig. 3c) also manifests in the $dln(R)/d\nu$ data, and $dln(R)/d\nu$ mostly maintains a positive value over the whole density range of the flat band.

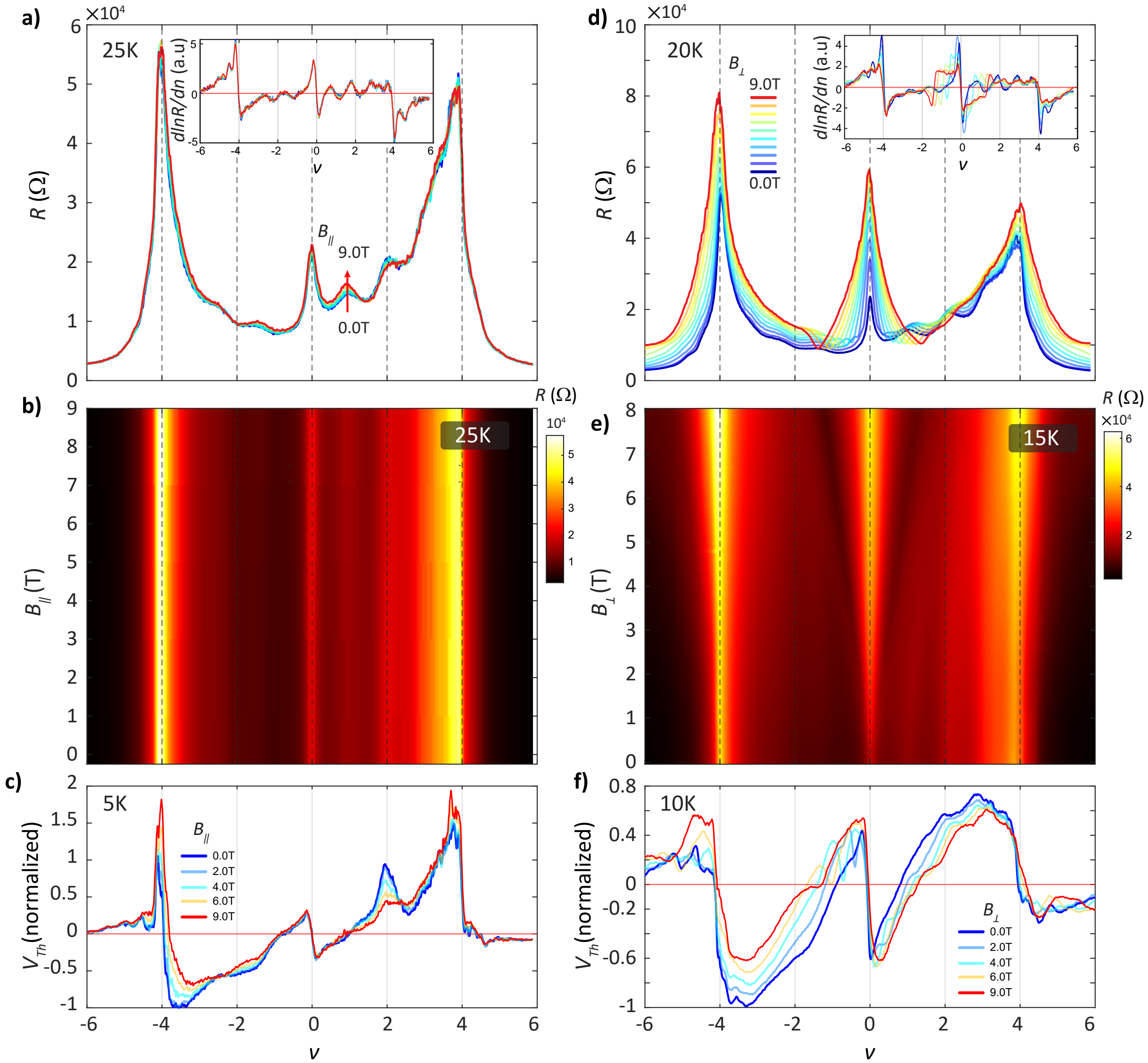

Extended Data Fig. 7: Resistance and thermoelectric voltage with in-plane and out-of-plane magnetic fields: **(a)** Resistance as a function of filling (ν) at different in-plane magnetic fields ($B_{||}$) at $25K$. Inset shows the $dln(R)/d\nu$ at corresponding $B_{||}$. **(b)** 2D plot of Resistance as a function of ν and in-plane magnetic field at $25K$. Clearly, no noticeable change can be observed in the resistance or $dln(R)/dn$ response, which starkly contrasts the V_{Th} response (see Figure 4 of the manuscript) with $B_{||}$. **(c)** Normalized V_{Th} with ν for different $B_{||}$ at $5K$. Here also, the significant reduction of V_{Th} is clearly visible with $B_{||}$. **(d)** Resistance as a function of ν at different out of-plane magnetic fields at $20K$. Inset shows the $dln(R)/d\nu$ at corresponding $B_\perp$. **(e)** 2D plot of Resistance as a function of ν and out of-plane magnetic field at $15K$. Except around the Dirac point, the signature of Landau levels can hardly be seen. The Mott formula, i.e., $dln(R)/d\nu$, also fails to capture any decrement with $B_\perp$ seen in Figure 4 in the main manuscript. **(f)** Evolution of normalized V_{Th} with $B_\perp$ at $10K$. Reduction of $\sim 40\%$ in V_{Th} at $\nu \simeq -3$ is apparent.

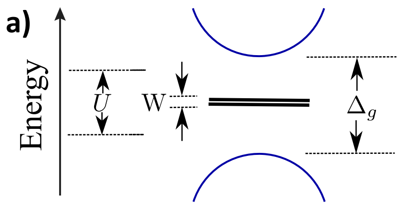

b)

Temperature scales	Theoretical V_{Th}	Characteristic Behavior	Experimental V_{Th}
$K_BT > \Delta_g$	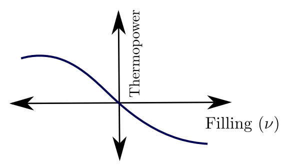	>0 for v<0 and <0 for v>0	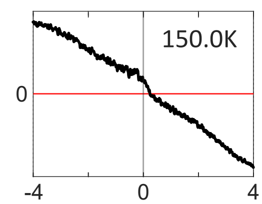
$U < K_BT \approx \Delta_g$	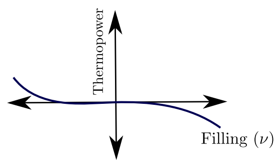	~0 in a range of v	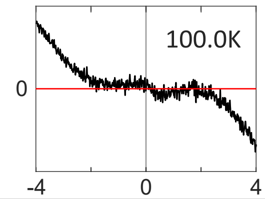
$U \lesssim K_BT < \Delta_g$	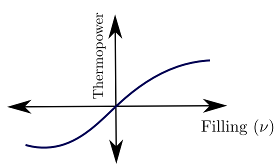	<0 for v<0 and >0 for v>0	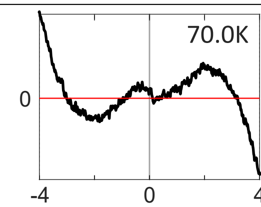
$K_BT < U$	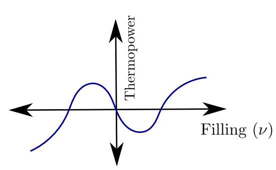	Threeprominent crossings	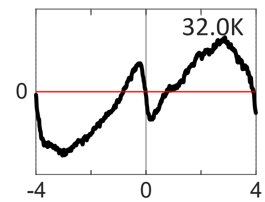

Extended Data Fig. 8: Comparison between the measured V_{Th} and expected theoretical thermopower at different temperature regime: (a) The key energy scales are bandwidth (W) of the flatband, the interaction strength (U), and the energy gap between the dispersing lower and upper bands (Δ_g). **(b)** (i) For $k_BT > \Delta_g$; the high-temperature thermopower is positive for $\nu < 0$ and negative for $\nu > 0$ (as depicted in the 1st row). A characteristic of graphene-based systems where electron-hole symmetry renders one crossing at $\nu = 0$ (Dirac point). (ii) For $U < k_BT \approx \Delta_g$; the effect of flat bands starts contributing together with higher dispersing bands. However, both contributions have opposite signs, resulting in almost flat, close to zero V_{Th} (as shown in the second row). (iii) For $U \approx k_BT < \Delta_g$; in this regime, the effect of the flatbands dominates over the higher energy bands. This leads to entropy being maximum at $\nu = 0$ and single thermopower crossing at $\nu = 0$ with positive for $\nu > 0$ and negative for $\nu < 0$ (as depicted in the third row). (iv) $U < k_BT$; the interaction dominates and dictates the entropy, which results in three prominent crossings (as shown in the last row), and discussed in Extended data Fig. 9.

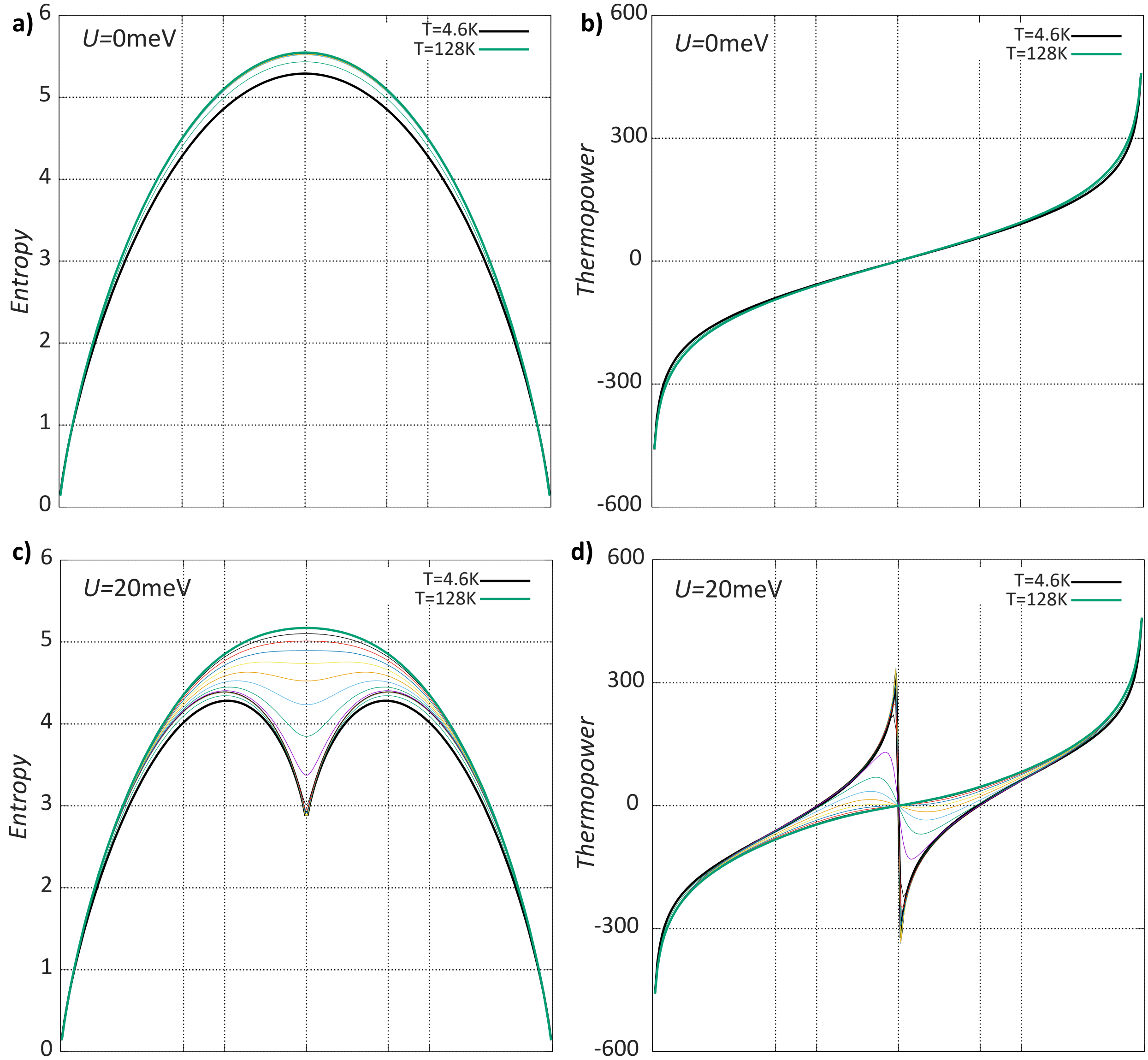

Extended Data Fig. 9: **(a), (b)** Behavior of entropy and thermopower for the four orbital atomic limit, where the onsite energies are $-\epsilon_1 = -\epsilon_2 = \epsilon_3 = \epsilon_4 = 0.2meV$, and Hubbard interaction $U = 0meV$. Different curves correspond to different temperatures: 4.6K, 7K, 14K, 16K, 19K, 21K, 23K, 26K, 35K, 46K, 58K, 70K, 81K, 93K, 104K, 116K and 128K. Thermopower has a zero crossing at only $\nu = 0$. **(c),(d)** Behavior of entropy and thermopower for the four orbital atomic limit where the onsite energies are $-\epsilon_1 = -\epsilon_2 = \epsilon_3 = \epsilon_4 = 0.2meV$, Hubbard interaction $U = 20meV$. Different curves correspond to different temperatures: 4.6K, 7K, 14K, 16K, 19K, 21K, 23K, 26K, 35K, 46K, 58K, 70K, 81K, 93K, 104K, 116K and 128K. Thermopower has a zero crossing at $\nu = 0$ and $\pm\frac{4}{3}$.